Extracellular modulation of TREK-2 activity with nanobodies provides insight into the mechanisms of K2P channel regulation

Karin E.J. Rödström[1,2,3,4], Alexander Cloake[1]*, Janina Sörmann[1,2]*, Agnese Baronina[3*], Kathryn H.M. Smith[1,2,4], Ashley C.W. Pike[3], Jackie Ang[3], Peter Proks[1,2], Marcus Schewe[5], Ingelise Holland-Kaye[4], Simon R. Bushell[3], Jenna Elliott[1], Els Pardon[6,7], Thomas Baukrowitz[5], Raymond J. Owens[8,9], Simon Newstead[2,4,10], Jan Steyaert[6,7], Elisabeth P. Carpenter[3,10#] and Stephen J. Tucker[1,2,10#]*

*Contributed equally

[#]To whom correspondence should be addressed:

stephen.tucker@physics.ox.ac.uk

lizcarpen1@gmail.com

1: Clarendon Laboratory, Department of Physics, University of Oxford, UK

2: Kavli Institute for Nanoscience Discovery, University of Oxford, UK

3: Centre for Medicines Discovery, University of Oxford, UK

4: Department of Biochemistry, University of Oxford, UK

5: Institute of Physiology, Medical Faculty, Kiel University, Kiel, Germany

6: Structural Biology Brussels, Vrije Universiteit Brussel, Brussels, Belgium.

7: VIB-VUB Center for Structural Biology, VIB, Brussels, Belgium.

8. The Rosalind Franklin Institute, Harwell Campus, Didcot, UK.

9. Division of Structural Biology, University of Oxford, Oxford, UK.

10: OXION Initiative in Ion Channels and Disease, University of Oxford, UK

Abstract

Potassium channels of the Two-Pore Domain (K2P) subfamily, *KCNK1-KCNK18*, play crucial roles in controlling the electrical activity of many different cell types and represent attractive therapeutic targets. However, the identification of highly selective small molecule drugs against these channels has been challenging due to the high degree of structural and functional conservation that exists not only between K2P channels, but across the whole K^+ channel superfamily. To address the issue of selectivity, we generated camelid antibody fragments (nanobodies) against the TREK-2 (*KCNK10*) K2P K^+ channel and identified selective binders including several that directly modulate channel activity. X-ray crystallography and CryoEM data of these nanobodies in complex with TREK-2 also reveal insights into their mechanisms of activation and inhibition via binding to the extracellular loops and Cap domain, as well as their suitability for immunodetection. It also facilitated design of a biparatropic inhibitory nanobody with markedly improved affinity and efficacy. These new tools therefore provide important insights into TREK channel gating and suggest alternative, highly selective approach to modulation of K2P channel activity via their extracellular domains.

Introduction

Ion channels control or contribute to the electrical activity and function of almost every living cell. Their selective pharmacological manipulation therefore offers wide-ranging approaches to plant, animal and human health[1]. In particular, the regulation of K^+-selective ion channels presents therapeutic potential for a wide variety of human disorders including epilepsy, arrhythmias and various other cardiovascular diseases and neurological conditions, especially the control of pain. Significant effort has therefore been expended in the identification of drugs that target specific types of K^+ channels for the treatment of such disorders[2, 3].

However, although there are over 80 different K^+ channel genes in the human genome, most have a similar architecture in their pore region because this highly conserved structural feature facilitates the selective permeation of K^+ as well as some of the conserved gating mechanisms they employ. As a consequence, the identification of highly selective small molecule agonists and/or antagonists that exhibit no cross-reactivity with other K^+ channels is challenging[1, 4].

Two-Pore Domain K^+ channels (K2P) are a distinct subset of K^+ channels where each gene encodes a subunit with two pore-forming domains that dimerise to create a single pseudotetrameric K^+ selective channel across the membrane [5]. These channels underlie the background K^+ currents that control the membrane potential in many different cell types where their activity is often regulated by diverse stimuli[6]. In particular, the TREK subfamily of K2P channels (TREK-1, TREK-2 and TRAAK) are regulated by a wide variety of physical and chemical stimuli. This polymodal regulation allows them to integrate cellular electrical activity with a diverse range of cellular signalling pathways[2, 7].

A number of structures now exist for members of the TREK subfamily that has allowed detailed gating models to be proposed[4, 8-11]. Like many other K^+ channels, movement of the pore-lining helices, in particular the M4 helix appears important for the regulation of TREK channel gating. However, unlike many other K^+ channels these movements do not constrict a lower ‘bundle-crossing-like’ gate at the cytoplasmic entrance to the pore. Instead, the channel appears to be gated primarily by much smaller structural changes in the selectivity filter with the ‘M4 Up’ conformation supporting a more active state of the channel than the M4 down conformations. However, there is evidence that the channel can support K^+ conduction in both conformations[12, 13]. Recent evidence suggests that the movement of M4 couples to the filter gate via changes in the network

of interactions that support the selectivity filter in its activated state[14].

The expression of TREK channels within the central and peripheral nervous systems[7] and their involvement in processes such as pain perception, neuroprotection, and anaesthesia makes them attractive therapeutic targets[2, 15]. Recent approaches have focused on the development of TREK channel agonists as potential analgesics and several lead compounds have been identified that target different elements of the gating mechanism within the selectivity filter of the channel[4, 11, 16]. However, although such small molecules have proven to be highly effective agonists, and much is now known about their mechanism of action, they often exhibit cross reactivity within the TREK subfamily. Also, in many cases, these agonists activate other classes of K^+ channel thereby limiting their potential use[4]. Other approaches to target these channels may therefore be required.

For some classes of ion channels, the adaptation of channel toxins and the development of RNA-based antagonists has been successful in achieving greater target selectivity[17, 18], but perhaps the most promising approaches involve biologics that exploit protein-protein interactions for target recognition[19-22]. Many antibody-based therapies are now in clinical use for the treatment of a variety of disorders and have a number of potential benefits compared to traditional approaches although their identification and development can be costly[23].

Nanobodies are single-domain (V_{HH}) antibodies derived from camelid heavy chain antibodies[24]. Their name derives from their small size and when compared to small molecule inhibitors, have certain advantages such as high target specificity and low toxicity leading to fewer off-target effects[25]. In addition, their small size and long complementarity determining region 3 (CDR3) loops enable them to access cavities or clefts in proteins that are inaccessible to antibodies[26].

They can also exhibit greater stability and solubility than conventional antibodies, so when combined with their relative ease of production, purification and engineering, this makes them ideal candidates for many therapeutic strategies where small molecule approaches have stalled[27], as well as equivalent detection surrogates for antibodies in immunocytochemistry[28]. They are also particularly useful probes to study structure-function relationships and other properties of ion channels and membrane proteins in general[29].

In this study we have generated a range of nanobody binders to the TREK-2 K2P channel, several of which exhibited highly specific regulation of channel activity. Our results also permitted design of a biparatropic inhibitory nanobody targeting spatially discrete epitopes which exhibited markedly improved efficacy. The insights provided by these nanobodies highlight new mechanistic approaches to the study of K2P channels and their role *in vivo*, and expand the potential of nanobodies as therapeutic agents.

Results and Discussion

Generation of TREK-2 nanobodies. Nanobodies were produced as part of the Nanobodies4Instruct program in a method described by Pardon *et al.*[30]. Briefly, purified human TREK-2 protein, identical to that used in previous structural studies[9] was used to elicit an immune response in llamas. The resulting immune repertoire was isolated and positive clones selected by phage panning and screening against the same TREK-2 protein. Overall, a panel of 29 unique nanobodies were produced (**Supplementary Fig. S1**) and these were further examined for their ability to produce a peak shift on size exclusion chromatography (SEC) to determine which nanobodies were capable of forming tight complexes (**Fig. 1A**). These tight binders were considered more suitable for subsequent structural and/or functional applications.

Screening for functional effects. To determine possible functional effects of the nanobodies on channel activity, human TREK-2 channels were expressed in *Xenopus* oocytes and currents measured before and after extracellular addition of nanobody (0.5 μM). An increase (or decrease) in current size by more than 50% was used as the initial threshold in this screen. The results are shown in **Fig. 1A** and reveal that from this initial panel, three exhibited clear functional modulation of TREK-2: nanobody CA10761 inhibited channel activity, whilst CA10767 and CA10776 both activated TREK-2. Functional effects of these nanobodies were also consistent with their tight binding as determined in the SEC shift assay (**Fig. 1A**). These modulatory nanobodies were then selected for further structural studies. Another tight binder that exhibited no functional effect (CA10758) was also included.

Nanobody binding to the extracellular Cap domain. Structures of these four nanobodies in complex with TREK-2 were then determined by X-ray crystallography using approaches similar to those previously described [4, 9] and were resolved between

2.4 Å and 3.6 Å resolution. For clarity these nanobodies were also renamed to reflect their functional effect (**Fig. 1B and Supplementary Fig. S2 and Table S1**).

All four of these nanobodies exhibited binding to the extracellular Cap domain of TREK-2 (**Fig. 1B**). Interestingly, the functionally inactive binder only interacted with the extracellular tip of the Cap domain whilst the modulatory nanobodies interact with both the Cap and extracellular loops much closer to the selectivity filter where the primary gate is located. In one case (CA10767), binding was also observed to the intracellular face as well as the Cap domain. The properties of these structures and the functional effects of each modulatory nanobody are described in more detail below.

Immunodetection of TREK-2 expression at the cell surface. Previous studies have demonstrated the usefulness of nanobodies for immunodetection as well as in various immunoassays and other nanobody-based protein targeting strategies [19, 28]. The structures determined above show that these TREK-2 nanobodies bind to the extracellular Cap domain indicating that immunodetection of TREK-2 at the cell surface should be possible. To examine this, we chose the functionally inactive nanobody CA10758 which interacts with the most exposed tip of the Cap domain. This nanobody is hereafter referred to as Nb-Binder-58 (or Nb-58).

Many K2P channels exhibit N-linked glycosylation to their extracellular surfaces that may affect nanobody binding [31]. However, only one glycosylation site exists within TREK-2 in the extracellular loop that precedes Pore-Helix-1 (PH1). None of the four chosen nanobodies interact with, or near this loop. Instead, Nb-Binder-58 binds as a dimer to the very tip of the Cap domain where it interacts with several residues that are unique between TREK-2 and the closely related TREK-1 channel (**Fig. 2A**).

To determine whether this nanobody can detect TREK2 expression at the cell surface,

Nb-Binder-58 was fused to the mVenus fluorescent protein and applied to HEK-293 cells expressing TREK-2 tagged with the mCherry fluorescent protein. **Fig. 2B** shows overlapping signals that are not observed on cells expressing TREK-1, nor for any other K2P channel (**Supplementary Fig. S3**). A similar, functionally inactive nanobody (CA10757: Nb-Binder-57 or Nb57) that exhibits almost complete sequence identity with Nb-Binder-58 is also capable of similar immunodetection of TREK-2 (**Fig. 2B** and **Supplementary Figs. S1 & S3**). This indicates that both these nanobodies represent useful tools for the specific immunodetection of homomeric TREK-2 channels.

A partially-selective activatory nanobody. The first activatory nanobody (CA10767) hereafter referred to as Nb-Activator-67 (or Nb67), binds to the side of the Cap domain (**Fig. 3A**) with all three CDR loops interacting with the external face of the Cap helices. However, these interactions are not symmetrical and on one side the EH1 Cap helix is partially unwound at the midpoint (residues 107-109; **Fig. 3C**). The structure also reveals a nanobody bound to the intracellular side where it occludes the entrance to the inner cavity (**Fig. 3A**). However, upon closer examination of the crystal structure this 'intracellular' interaction appears to result from tetramerisation of the nanobody within the unit cell that may drive the crystal packing and the resulting non-canonical structure (**Supplementary Fig. S4A**). Nevertheless, to rule out any functional effects of this intracellular interaction we examined the effect of this nanobody on TREK-2 currents in excised patches where it could be applied to the intracellular surface of the membrane. No functional effect on TREK-2 activity was observed even at 10 μM intracellular application (**Supplementary Fig. S4B**). This is in marked contrast to its clear activatory effect when applied extracellularly (**Fig. 1A**). Further examination revealed that Nb-Activator-67 rapidly increased channel activity ~3-4 fold with nanomolar efficacy (EC_{50}= 101 ± 12 nM) when perfused onto oocytes expressing human TREK-2 (**Fig. 3B**).

To address its selectivity, we examined effects on other K2P channels. No functional modulation was observed on either TALK-2 or TRAAK. However, an inhibitory effect was observed on the closely related TREK-1 channel at high concentrations of nanobody >1μM (**Fig. 3B**). This opposite effect initially appeared interesting because of the opposite effects of extracellular pH on the activity of TREK-2 and TREK-1, and the role of the extracellular Pore/TM loops in this process[32]. However, Nb-Activator-67 does not appear to contact these loops and instead only interacts with the extracellular face of the Cap domain resulting in an unwinding of the EH1 Cap helix on one side (**Fig. 3C**). Intriguingly, both M4 helices in this TREK-2 structure are in the Up conformation consistent with a more activated state of the channel (**Fig. 3A**), although this could also be due to its interactions with the nanobody bound to its intracellular surface. Full occupancy of ion binding sites within the filter of TREK channels is also usually associated with an activated state of the channel[9, 33], and in this structure all the sites appear occupied, albeit in an asymmetric fashion due to unwinding of the Cap on one side (**Fig. 3A**). Although it is tempting to associate the effect of unwinding of EH1 with the activatory effects of Nb-Activator-67, the crystal packing interactions make interpretation of this particular structure challenging. Due to the additional lack of specificity between TREK-1 and TREK-2, the mechanism of activation by this nanobody was not investigated further. However, its robust activatory effect on recombinant homomeric TREK-2 channels, especially at lower concentrations, indicates that this nanobody may remain a useful tool in situations where the identity of its target is already known.

A selective activatory nanobody. Unlike Nb-Activator-67, the second activatory nanobody (CA10776, hereafter referred to as Nb-Activator-76 or Nb76) exhibited highly selective activation of TREK-2 with an efficacy of 412 ± 14 nM and had no effect on TREK-1 or other K2P channels tested, even when used at high concentration (**Fig. 4A**

& **Supplementary Fig. S4C**). The structure of this nanobody in complex with TREK-2 reveals that the CDR loops interact with the side of the Cap domain involving residues at the intersubunit interface (**Fig. 4B, C**). In particular, W98 on CDR3 of the nanobody inserts into the intersubunit groove between helices in the Cap domain of TREK-2 to form an interaction with E128 (**Fig. 4C**). R53 on CDR2 also helps anchor the nanobody to the Cap helices by H-bonding with Q106 on TREK2 **(Fig. 4C)**. Consistent with this, we found that mutation of either of these residues on Nb-Activator-76 (W98A or R53A) severely impaired its activatory effect (**Fig. 4A**).

Nb-Activator-76 also contacts the extracellular P2-M4 loop. In particular, N56 on CDR2 interacts with N292 on the P2-M4 loop of TREK-2 (**Fig. 4D**). This extracellular loop has previously been implicated in the regulation of filter-gating by external H^+ [32]. The importance of this interaction with the P2-M4 loop is confirmed by mutation of N56 on Nb-Activator-76 which reduces its activatory effect, (**Fig. 4A**). Consistent with an activated state, both M4 helices in this structure are also in the Up conformation (**Fig. 4F)**. The role of ions in gating the filter is unclear because crystals of sufficient quality could only be obtained using a crystallisation solution containing Ba^{2+} which contributes to the crystal contacts. However, this does not change the selectivity filter in comparison to the Up-state conformation (PDB ID 4BW5).

ML335 is a small molecule TREK channel agonist that binds within the 'K2P Modulator Pocket', a cryptic binding site created by displacement of the top of M4 where its interactions with the P2-M4 loop and Pore-Helix-1 (PH1) are proposed to stabilise TREK-2 in a more conductive conformation[11, 16, 34]. It is therefore highly significant that interaction of Nb-Activator-76 with the P2-M4 loop also induces a displacement in the top of the M4 helix similar to that seen in the ML335-bound structures of TREK-2 (**Fig. 4E**). Furthermore, it has been reported that the reorientation of a tryptophan residue at

the top of M4 (W306 in TREK-2) also correlates with the activated state of TREK channels[8, 10, 35] and that any hydrophobic moiety occupying this space is capable of stabilising this activated state[10]. In this nanobody-bound structure W306 sidechains in both helices are in the inward orientation and occupy this space. But unlike other TREK structures where this M4 tryptophan has rotated inwards, here the adjacent residues on PH1 (F164) also flips orientation to interact with the top of M4 to stabilise this displacement (**Fig. 4F**). This demonstrates a mechanism whereby movement of the M4 helix may communicate with PH1 to influence the selectivity filter gate and highlights the importance of this 'K2P modulator pocket' in channel gating [36].

An inhibitory nanobody with dual effects. The inhibitory nanobody, CA10761, hereafter referred to as Nb-Inhibitor-61 (or Nb61), rapidly inhibited TREK-2 currents (IC_{50} = 685 ± 18 nM; **Fig. 5A**). Its structure in complex with TREK-2 indicates only one nanobody bound per asymmetric unit, but this appears to result from its crystal packing where interactions between the Cap domains prevent binding of a second nanobody to the opposite side (**Fig. 5B).**

The position of Nb-Inhibitor-61 on the side of the Cap domain allows it to form extensive interactions between the Cap helices and CDR1, as well as with the β5 sheet and β5-β6 loop. In addition, its long CDR3 loop forms multiple interactions with the top of M3 and the M3-PH2 loop (**Fig. 5C**) as well as additional interactions with the top of M2 and the P2-M4 loop. However, the most striking feature of this long CDR3 loop is that it also inserts a lysine residue (K103) deep within the extracellular ion exit pathway that emerges just below the Cap domain (**Fig. 5E-F**). Overall, the position of this nanobody obstructs most of this ion exit pathway with the remaining gap being only 1.35 Å wide compared to > 4 Å in the *apo* state. Intriguingly, the position of this positively-charged lysine within the ion exit pathway is reminiscent of the way some toxins block K^+

channels via a “cork in a bottle” or “plug” type mechanism[37]. It also shares similarities with the ‘finger in the dam’ mechanism of TREK channel block by Ruthenium Red where interaction of this the positively-charged inhibitor with the ‘keystone inhibitor site’ below the Cap domain directly blocks K^+ permeation[7, 36, 38]. Unlike these other toxins, K103 does not insert far enough into the pathway to interact directly with ions exiting the filter, but it clearly has the ability to impede K^+ movement through this exit pathway and so we examined its role further.

A critical role for Lysine 103 in channel inhibition. This lysine appears to make no specific H-bonding or charged interactions within the ion exit pathway and mutation to a serine (K103S) resulted in a marked reduction in its inhibitory effect (**Fig. 5A**). We also examined other substitutions at this position (K103R, K103N and K103D). Consistent with a role for a positively charged residue at this position, the K103R mutant produced similar, if not greater, inhibition whilst neutral or negative substitutions (K103N and K103D) resulted in a markedly reduced inhibitory effect (**Fig. 5A**). We also examined the effect of this nanobody on TREK-2 activity at the single channel level (**Supplementary Fig. S5**). Due to the low intrinsic open-probability of TREK-2, only a qualitative comparison was made between the behaviour of multi-channel patches with or without Nb-Inhibitor-61 included in the pipette solution. This revealed a marked suppression of TREK-2 activity via reduction in the durations of bursts of openings and increase in the time spent in the long-closed states. This is consistent with the idea that this nanobody acts as a slow blocker resulting in a complete cessation of K^+ flux through the channel.

Possible allosteric effects of Nb-Inhibitor-61 Together, these results with Nb-Inhibitor-61 support the contribution of a direct toxin-like (or ‘finger in the dam’) block of ion permeation by the nanobody[38]. However, the bifurcation of the ion exit pathway

means that such a mechanism would also require nanobody binding to both sides of the Cap domain. There are no obstructions to the binding of a second nanobody on the other side, but due to crystal packing only one is observed in this structure. It is therefore possible that other, allosteric mechanisms may also contribute to its inhibitory properties. For example, multiple effects are also seen in some toxins where, in addition to direct pore block, interactions with the external pore loops result in allosteric modulation of channel gating[39, 40]. For Nb-Inhibitor-61, this may arise through the extensive contacts it makes with the M3-PH2 loop as well as with the P2-M4 loop and M2/M3 helices. Consistent with such an allosteric effect, the M4 helix of the subunit that interacts with this nanobody is in the Down conformation (**Fig. 5B**). Furthermore, the relative orientation of side chains for both W306 on M4 and F164 on PH1 are reversed compared to their positions the Nb76/TREK-2 structure, and its interaction with the P2-M4 loop pulls the top of M4 closer to PH1 compared to the activated state induced by Nb-Activator-76 (**Fig. 4F**). However, all 4 ion binding sites in the filter appear to be occupied and no obvious structural changes are seen in this region. Thus, although additional allosteric effects of this nanobody on the filter gate cannot be excluded, Lysine 103 clearly contributes to channel inhibition by directly blocking the ion exit pathway.

A biparatopic inhibitory nanobody with improved efficacy The two activatory nanobodies identified in this study function with relatively high efficacy (EC_{50} ~100 & 300 nM) compared to Nb-Inhibitor-61 (IC_{50} ~650 nM). Multivalency is a well-established method for increasing the affinity of ligands, and linked biparatopic nanobodies which target spatially discrete epitopes have also proven an effective way of increasing their functional efficacy[41, 42].

We therefore attempted to increase the efficacy of Nb-Inhibitor-61 by linking it to the

non-functional Cap binder (Nb-Binder-58). Comparison of the TREK-2/Nanobody structures (**Fig. 1B**) revealed non-overlapping binding sites for these two nanobodies with a distance of ~21 Å between the C-terminus of Nb-Inhibitor-61 and the N-terminus of Nb-Binder-58. The two were therefore linked in frame with a $(Gly\text{-}Ser)_4$ linker to create a divalent biparatopic nanobody we refer to as Nb-Inhibitor-6158 (or Nb-6158).

Analysis of the relative binding affinity of this biparatopic nanobody using biolayer interferometry revealed a marked increase in affinity for TREK-2 of at least 250-fold (4.1 ± 0.1 nM, *n*=4) compared to monomeric Nb-inhibitor-61 (1100 ± 30 nM, *n*=4;). This was also reflected in a 16-fold increase in its inhibitory efficacy from 651 ± 18 nM to 40 ± 3 nM, *n=5* (**Fig. 6A**).

Nb-Binder-58 binds as a dimer to the Cap domain suggesting that two copies of Nb-Inhibitor-61 in this biparatropic nanobody may now be able to bind more efficiently and directly occlude both ion exit pathways. Given the arrangement of the unit cell in the crystal structure of the TREK-2/Nb61 complex we attempted to determine its structure in complex with TREK-2 by cryo electron microscopy (**Fig. 6B** and **Supplementary Fig. S6**). At ~7.4Å resolution, the map was sufficient to reveal two copies of Nb-Inhibitor-6158 bound with one Nb-Inhibitor-61 domain on either side of the Cap domain similar to its position in the crystal structure. This confirms that this nanobody can interact with both subunits of TREK-2 to exert allosteric effects as well as occluding both extracellular ion exit pathways.

Summary and Conclusions

In this study, we describe the generation and characterisation of a panel of nanobody binders to the TREK-2 K2P channel resulting in one inhibitor, two activators and other nanobodies suitable for immunodetection of TREK-2. One activator in particular (Nb-

Activator-76) elicits highly selective activation of TREK-2. These nanobodies therefore not only provide useful probes for analysing the structure and function of homomeric TREK-2 channels, but also identify a new class of highly specific extracellular modulators that can be further investigated for therapeutic potential.

Ever since the first structures of K2P channels were resolved over a decade ago the role of their large extracellular Cap domain has remained unclear[33, 43]. It was initially suggested this domain may have evolved to protect the selectivity filter of K2P channels from the small peptide toxins that often target other members of the superfamily of tetrameric cation channels. However, the complex domain swap involving the M1 helix required to assemble this extracellular domain suggests this is an unlikely strategy, especially as examples of toxin-resistance in ion channels often only require single mutations in the extracellular toxin binding site[44].

Nevertheless, the Cap domain is a defining feature of K2P channels, and whatever its purpose, it obviously makes toxin block of the pore much less likely. It is therefore significant that we have identified a nanobody in which the longer CDR3 loop inserts a lysine sidechain directly into the extracellular ion exit pathway in a manner analogous to some K^+ channel toxins. In the case of TREK channel inhibition by Ruthenium Red, this small positively charged inhibitor is able to access deeper into the exit pathway to block permeation directly above the filter, whereas it may not be possible for this CDR3 loop to insert deep enough to access the keystone Inhibitor site, even if it were longer. Nevertheless, this inhibitory nanobody is highly effective and its mechanism of action likely involves both allosteric and direct blocking effects on permeation[13]. Also, the structure of this TREK-2/nanobody complex, and those of the others solved in this study, reveal that the Cap domain is highly immunogenic and provides a good scaffold on which nanobodies can anchor themselves to influence TREK channel function. We also

demonstrate that the Cap domain offers the opportunity for the design of biparatropic nanobodies with improved affinity and functional efficacy. In addition, the nanomolar efficacy of the linked Nb-inhibitor-5861 now provides a powerful analytical tool for probing TREK-2 function.

In the case of the two activators, the first (Nb-Activator-67) is a highly effective probe for the study of homomeric TREK-2 when the identity of the target is known, but uncertainties about this crystal structure make interpretations of its mechanism of action difficult. However, the second activator (Nb-Activator-76) provides important insights into the mechanism of TREK channel activation and demonstrate how the extracellular P2-M4 loop and rearrangements at the top of the M4 helix play a critical role in the regulation of channel gating. Overall, these rearrangements expand current models for TREK channel gating via the K2P modulator site to suggest that outward displacement of the top of M4 changes the contacts between M4, the P2-M4 loop and Pore-Helix-1 to activate the selectivity filter gate, whereas displacement in the other direction results in the opposite effect and inhibition. Similar to that proposed for other TREK channel modulators[8, 10, 16], this may also involve reorientation of the W306 and F164 side-chains, or their equivalents (**Fig. 7**). This model is also consistent with recent observations that covalent attachment of ML335 derivatives within the K2P modulator site via a conserved serine on PH1 can irreversibly activate TREK channels [34].

However, the mechanism by which nanobody binding is then coupled to changes in ion occupancy within the filter and the dynamics of K^+ permeation remain unclear. A limitation of this study is that the relative dynamics of these specific regions are probably critical for the regulation of gating, but most structures, including those in this study are determined in high [K^+] (>100 mM). This often results in high ion occupancy within the filter in such crystal structures, whereas the physiological situation is obviously very

different and difficult to compare.

The nanobody ‘binders’ that have no functional effects are also likely to be useful tools for the immunodetection of TREK-2, although future studies will be required to demonstrate the sensitivity required for detection *in vivo*. It is also known that TREK-2 can form heteromeric channels with either TREK-1 or TRAAK, and nanobodies capable of detecting such combinations would be extremely powerful for dissecting the role of such heteromeric channels *in vivo*. It is therefore significant that the domain swap involved in assembly of the Cap domain generates an intersubunit interface that forms extensive contacts with nanobodies in these structures and which would be unique in any heteromeric channel combinations; thus, if binders can differentiate between these interfaces in homomeric TREK channels, then it may be possible to generate similar nanobodies that are uniquely selective for heteromeric K2P channels.

Thus, although ion channels remain underexploited as antibody drug targets, this study demonstrates that the unique nature of the Cap domain combined with the role of the extracellular loops in K2P channels allows nanobodies to be considered as an exciting alternative to small molecules as highly-selective probes to K2P channel structure-function studies, and of TREK channels in particular. This therefore expands the potential of nanobodies as effective therapeutics and their role in future drug development.

Acknowledgments

We acknowledge the support and use of resources of Instruct-ERIC (PID1212 VID1054), part of the European Strategy Forum on Research Infrastructures (ESFRI) and the Research Foundation - Flanders (FWO) for support with nanobody discovery and thank Nele Buys for the technical assistance during Nanobody discovery. We also thank Diamond Light Source for beam time (BAG proposal mx15433/mx19301) and the I24 beamline staff for assistance with crystal screening and data collection, as well as the staff of the Central Oxford Structural Molecular Imaging Centre (COSMIC) for assistance with CryoEM. This work was supported by grants from the Biotechnology and Biological Sciences Research Council and Medical Research Council to S.J.T (BB/T002018/1, BB/S008608/1 and MR/W017741/1) and from the Deutsche Forschungsgemeinschaft to M.S. (SCHE 2112/1-2) and T.B (BA 1793/6-2) as part of the Research Unit FOR2518, DynIon. EPC was supported by the Structural Genomics Consortium, a registered charity (number 1097737) that received funds from AbbVie, Bayer, Boehringer Ingelheim, Genome Canada, Janssen, Merck, Novartis, the Ontario Ministry of Economic Development, Pfizer, and Takeda, as well as the Wellcome Trust (106169/Z/14/Z). S.J.T and E.P.C also received support from the Wellcome Trust as part of the OXION Initiatives in Ion Channels and Membrane Transport in Health and Disease (WT084655MA and 102161/B/13/Z).

Author contributions

S.J.T., E.P.C. and K.E.J.R. conceived/designed the principal elements of the study. All authors generated, analyzed or interpreted data or generated materials. E.P. and J.S. generated nanobody reagents. S.J.T, A.C., J.S. and K.E.J.R drafted the manuscript and all authors contributed to the final version.

Conflicts of interest

The authors declare no competing financial interest.

Data Availability

All data within this study are included in the article and/or the Supplementary Information. The atomic coordinates and structure factors for the nanobody bound complexes of TREK-2 have been deposited in the Protein Data Bank, www.pdb.org [PDB ID codes: 8QZ1 (Nb58), 8QZ2 (Nb61), 8QZ3 (Nb67), 8QZ4 (Nb76)]. Electron density for the biparatropic Nb6158 is deposited at the Electron Microscopy Data Bank with the entry ID code, EMD-19066.

Methods

Nanobody generation, expression and purification: Nanobodies were generated as part of the Nanobodies4Instruct program using the method described by Pardon *et al.* (28). Briefly, detergent-solubilised purified human TREK-2 protein (Gly67 to Glu340), identical to that used in previous structural studies (9) was used to elicit an immune response in llamas. The resulting immune repertoire was isolated and cloned into the pMESy4 phage display vector. Positive clones were selected by phage panning and screening against the same TREK-2 protein. A total of 29 unique nanobody clones were identified. The sequence alignments shown in **Supplementary Fig. S1** are highlighted using TEXshade. To create the biparatropic Nb6158, extension overlap PCR was used to link the C terminus of Nb61 to the N terminus of Nb58 with a $(GGGGS)_3$ linker. Periplasmic expression and purification were modified from Pardon *et al*. [30]. Briefly, relevant nanobodies in the pMESy4 vector which has a N terminal PelB signal sequence and a C terminal 6x-His tag. These were transformed into the WK6 strain of *E. coli*. 10

ml overnight cultures were then used to inoculate master cultures (1L Terrific Broth, 4ml Glycerol, 0.1 % w:v glucose). These were then grown at 37 °C shaking at 180 rpm with expression induced by 0.5mM IPTG when OD_{600} reached 0.8. Growth was then continued overnight at 28 °C. Cells were harvested by spinning at 5000g for 20 minutes at 4 °C and the pellets resuspended in ice-cold resuspension buffer (in mM: 200 Tris, 0.5 EDTA, 500 Sucrose). To disrupt the periplasm, cells were kept on ice and shaken for 1 hour in resuspension buffer, followed by a rapid 3-fold dilution with a 5mM $MgCl_2$ solution and then shaken for a further hour. The periplasm was then recovered by spinning at 15000 *g*, for 15 mins at 4 °C. His-tagged nanobodies were then purified by addition of Ni-NTA resin to the supernatant and incubating at 4 °C for 2.5 hours. Following washing with Wash Buffer 1 (in mM: 50 Sodium Phosphate, 1000 NaCl, pH7.0) and Wash Buffer 2 (in mM: 50 Sodium Phosphate, 1000 NaCl, pH6.0), nanobodies were eluted in Elution buffer (in mM: 50 Sodium Phosphate, 150 NaCl, 300 Imidazole, pH 7.0, and the imidazole rich solution exchanged into either Gel Filtration Buffer (200 mM KCl 20 mM HEPES pH7.5, for screening experiments), ND96 (in mM: 96 NaCl, 2 KCl, 1.8 $CaCl_2$, 1 $MgCl_2$, 20 HEPES, 2.5 Na Pyruvate, for Two-Electrode Voltage Clamp studies), or extracellular buffer (in mM: 140 NaCl, 10 TEA-Cl, 5 KCl, 3 MgCl, 1 $CaCl_2$,10 HEPES, pH 7.4, for patch clamp electrophysiology) using PD10 columns. Purity was assessed by SDS-PAGE. An initial assessment of nanobody binding to TREK-2 was done with size exclusion chromatography. Each nanobody was mixed with purified TREK-2 in a 2:1 molar ratio and applied to a Sepax SRT SEC-300 column, pre-equilibrated in Gel Filtration buffer. Out of the 29 initial nanobodies, 16 co-eluted with TREK-2 and produced a visible shift of the 280 nm TREK-2 peak, compared to TREK-2 injected without nanobody.

Crystallography and Data Collection Human TREK-2 protein (residues Gly67 to Glu340), identical to that used in our recent structural studies was expressed and

purified as previously described [4, 9] and relevant nanobodies were prepared as described above. For Nb67 and Nb61 a TREK-2 glycosylation mutant (TREK-2^{glyco}) was used; this was purified in an identical manner and contained the following substitutions (N149Q, N152Q and N153Q; none of these sites form contacts with the nanobody). TREK-2 protein was mixed with the nanobody in a 1:2 TREK-2:nanobody molar ratio prior to crystallisation. Crystals formed in vapour diffusion drops (TREK-2-Nb58: 0.1 M glycine pH 10.0, 0.2 M NaCl, 31% v/v polyethylene glycol (PEG) 1000; TREK-2^{glyco}-Nb67: 0.1 M Tris pH 8.0, 65% v/v 2-methyl-2,4-pentanediol; TREK-2-Nb76: 0.1 M HEPES pH 7.0, 0.3 M $BaCl_2$, 39% PEG 400), apart from the TREK-2^{glyco}-Nb61 complex crystals, which grew in Lipidic Cubic Phase (MAG7.9 with 3:2 lipid:protein ratio, 0.1 M Na acetate pH 4.5, 0.3 M KCl, 23% v/v PEG 400). Vapour diffusion crystals were grown at 4°C and LCP crystals at 20°C for 1-12 weeks. Crystals were screened, and X-ray diffraction data collected on beamline I24 (Diamond Light Source) at 100K. Data were recorded at a wavelength of 0.9686Å on a Pilatus3 6M detector from single crystals using 0.1 or 0.2° oscillation and a beam-size of 20x20μm (30x30μm for TREK-2-Nb76). Data were processed, reduced and scaled using XDS [45] and AIMLESS [46]. All datasets exhibited moderate to strong diffraction anisotropy and were further processed using STARANISO (http://staraniso.globalphasing.org) to apply an anisotropic diffraction cut-off to the merged data as well as structure amplitude estimation and anisotropic correction (see **Supplementary Table S1** for resolution limits of data and completeness). Structures were phased by molecular replacement using the 4BW5 (TREK-2 ^{glyco}-Nb67 and TREK-2-Nb76), 4XDJ (TREK-2 ^{glyco}-Nb61) or 4XDK (TREK-2-Nb58) structures as starting models for TREK-2 [9] and 5HVG (Nb58 and Nb76), 5UKB (Nb67) or 5IMK (Nb61) for the nanobodies. Structures were manually built with COOT and refined with BUSTER (2.10.4; Global Phasing Ltd). Models were refined with LSSR restraints [47] and a single translation/libration/screw model group was refined for each

protein chain.

Cryo Electron Microscopy and Data Collection: Purified TREK2 was complexed with purified linked Nb6158 at a 1:1.2 molar ratio and incubated for 2h on ice. TREK2-Nb complex was separated from free Nb by gel filtration on a Superose 6 Increase column in 200 mM KCl, 20 mM HEPES pH 7.5 and 0.12% OGNG with 0.012% CHS. The complex was concentrated to 5.1mg/ml and a 3µl aliquot applied to a glow-discharged Quantifoil holey carbon grid (1.2/1.3 300 Cu mesh) and blotted for 3s (100% humidity, 4°C) using a VEI Vitrobot IV. Data was collected at the Central Oxford Structural Molecular Imaging Centre (COSMIC) on a FEI Arctica 200 kV cryo-TEM with FEI Falcon 4 direct electron detector. Movies were recorded at 150000x magnification with a pixel size of 0.94 Å per pixel and a total dose of 30 e-/Å^2. The defocus values ranged from -3.0 to -1.5 µm. Data was analysed using SIMPLE and CryoSPARC [48, 49]. In SIMPLE, manual picking was used to create 2D cluster templates to pick 301,660 particles from 2651 micrographs. The particles were exported to CryoSPARC and following two rounds of 2D classification and selection, 17,788 particles were selected for *ab-initio* reconstruction followed by homogeneous refinement to give a density map of 7.37 Å. A model was created by overlaying the crystal structures of TREK2 with Nb61 and Nb58. These were fitted in to the map in COOT[50] and further refined with PHENIX[51].

Biolayer interferometry: This was performed using an Octet Red385 (Sartorius). Streptavidin coated biosensors were loaded with biotinylated TREK2 at 50 nM in 200mM KCl, 20mM HEPES pH 7.5 and 0.12% OGNG with 0.012% CHS. To calculate K_d, serial dilutions of 2 µM to 7.8 nM for Nb 61 and 1000 nM to 3.9 nM for Nb6158 were prepared. After a 300 sec baseline step, the nanobodies were allowed to associated for 600 sec and then dissociate for 600 sec. Data was analysed in the Octet v9.0 software package and all raw data were filtered with a Savitzky-Golay filter, baseline and

reference subtracted, in-step corrected and y-axis aligned.

Immunodetection of TREK-2: TREK-2 and other human K2P channels were tagged with mCherry by removal of the stop codon and in frame fusion of mCherry to the C-terminus using a $(GS)_2$ linker and then cloned into the pFAW vector suitable for expression in HEK293 cells. Nanobodies were tagged by in frame fusion of mVenus at the C-terminus using a $(GS)_2$ linker, and also then cloned into the pFAW vector. The nanobody-mVenus fusions were then transfected into HEK293 cells resulting in secretion of tagged nanobodies into the media. This media was then harvested after 96 hours and used directly for immunodetection of mCherry-tagged K2P channels that had transfected into HEK293 cells at least 36hrs previously.

Electrophysiology: For microinjection of oocytes, mRNA was *in vitro* transcribed from the wild-type human TREK-2 gene (*KCNK10*) in the pFAW oocyte expression vector. Each oocyte was injected with ~0.2ng of RNA and Two-Electrode Voltage Clamp recordings then performed as previously described[12]. Briefly, after injection of mRNA, oocytes were incubated for 20–24 h at 17.5°C and measured in ND96 buffer at pH 7.4 (96 mM NaCl, 2 mM KCl, 2 mM MgCl2, 1.8 mM $CaCl_2$, 5 mM HEPES). Unless otherwise stated, for the dose-response measurements, oocytes were perfused with increasing concentrations of purified nanobody in ND96 solution and currents recorded using a 400 ms voltage step protocol from a holding potential of -80 mV delivered in 10 mV increments between -120 mV and +50 mV and 800 ms ramp protocols from -120 to +50 mV. Unless otherwise described, all results shown are reported as mean ± standard deviation and obtained with oocytes from at least 3 independent batches. For the initial screening experiments nanobody was pipetted directly into the bath chamber in gel filtration buffer and current recorded using a 800 ms ramp from -50 to +80 mV. For the measurement of intracellular effects, nanobodies were applied to the inside of giant

excised inside-out membrane patches. The intracellular solution had the following composition (in mM): 120 KCl, 10 HEPES, 2 EGTA and 1 Pyrophosphate (pH adjusted with KOH/HCl) with a pipette solution (in mM): 120 KCl, 10 HEPES and 3.6 $CaCl_2$ (pH 7.4 adjusted with KOH/HCl). The recording of TREK-2 channel activity was then performed as previously described[4]. For single channel recordings, the pipette solution contained (in mM) 116 NMDG, 4 KCl, 1 $MgCl_2$, 3.6 $CaCl_2$, 10 HEPES (pH 7.4); whilst bath solution contained (in mM) 120 KCl, 1 NaCl, 2 EGTA, 10 HEPES (pH 7.3). The currents were filtered at 1 kHz and sampled at 10 kHz.

Figure Legends

Figure 1. Identification of functionally-active nanobody binders for TREK-2 (A) Whole cell currents recorded (at +40mV) from oocytes expressing TREK-2 in the presence of a panel of nanobodies generated against TREK-2. Currents in the presence of extracellular nanobody (0.5 µM) were normalised to those in its absence. A threshold of 50% activation or inhibition was set in this screen (dotted lines). Tight binders within this panel were identified on the basis of producing a shift in size exclusion chromatography (SEC-shift) and shown in red. Asterisks mark the functionally active nanobodies plus an inactive tight binder chosen for further investigation. **(B)** Crystal structures of the three functionally active nanobodies in complex with TREK-2. The nanobodies are shown in purple as surface representations whilst TREK-2 is shown in cartoon (green and gold). For CA10767 (Nb-Activator-67) the third 'intracellular' nanobody in the unit cell is shown in grey. A structure of the functionally inactive binder, CA10758 (Nb-Binder-58) is also shown in complex with TREK-2. Note in this case that the nanobody binds as a dimer to the top of the Cap domain away from the extracellular TM/Pore loops that influence channel gating.

Figure 2. Nb-binder-58 interacts with the apex of the Cap domain. (A) Crystal structure of Nb-binder-58 (Nb58) in complex with TREK-2. This functionally inactive tight binder interacts as a dimer with the tip of the Cap domain only. The right-hand panel shows an expanded view of the interactions involved and shows the C123 disulphide between chains at the apex of the Cap. D120 and V122 are unique in TREK-2 compared to other TREK channels. **(B)** Immunodetection of TREK-2 at the cell surface. TREK-2-mCherry fusions were expressed in HEK293 cells and stained with either Nb58 (or the highly related Nb57) fused to mVenus. Overlay of these fluorescent signals shows clear binding at the extracellular surface. No overlapping signals are seen in untransfected controls or with other K2Ps (see **Supplementary Fig. S3**).

Figure 3. Extracellular activation of TREK-2 by Nb-Activator-67. (A) Crystal structure of TREK-2 in complex with Nb-Activator-67 (Nb67). Nanobodies bind to each side of the Cap domain and on one side (green subunit) the Cap helix unwinds. A third Nb67 (grey) is also found

in the asymmetric unit bound to the intracellular surface. These unusual features may arise from tetramerisation of Nb67 within the crystal (see **Supplementary Fig. 4A**) **(B)** Dose-response relationships showing extracellular activation of TREK-2 channel activity by Nb67. Whole-cell TREK-2 currents were recorded at +40 mV and perfused with different concentrations of Nb67. Currents were normalised to those recorded prior to the application of nanobody. No activation of TRAAK or TALK-2 K2P channels was observed, but for the related TREK-1 up to 50% inhibition of channel activity was seen at concentrations of Nb67 >1µM. **(C)** Expanded view of the interaction of Nb67 with the two sides of the Cap domain. The interaction with $Nb67_A$ (Left) shows no distortion of the helices, whereas interaction with $N67_B$ on the opposite side results in unwinding of $EH1_B$ (residues E113, E116 and D120 are unique in TREK-2 vs TREK-1). Right: the interaction of N108 with $NB67_B$ differs on the side where $EH1_B$ is unwound. This interaction does not occur with $Nb67_A$.

Figure 4. Selective extracellular activation of TREK-2 by Nb-Activator-76 **(A)** Dose-response relationships showing activation of TREK-2 channel activity by Nb-Activator-76 (Nb76). Whole-cell TREK-2 currents were recorded at +40 mV and perfused with different concentrations of Nb76. The effect of mutating different residues in Nb76, which interact with TREK-2, are shown. The curves shown for the R53A and W98A mutant nanobodies were fitted by hand. **(B)** Crystal structure of TREK-2 in complex with Nb76 bound to both sides of the Cap and the P2-M4 loop. **(C)** Interactions with the side of the Cap. W98 on CDR3 inserts between Cap helices of different TREK-2 subunits to form an interaction with E128 on EH2 of TREK-2, whilst R53 on Nb76 interacts with Q106 on EH1 of a different subunit of TREK-2. Mutation of either W98 or R53 on Nb76 reduces its activatory effect. **(D)** Expanded view of the interaction of N56 on CDR3 with N292 on the P2-M4 loop. Mutation of N56 also reduces activation by Nb76. **(E)** Alignment with TREK-2 Up state (4BW5 in Grey) highlights displacement of the top of M4 and the inward rotation of W306. This is accompanied by outward rotation of F164 on Pore-Helix-1 (PH1). The right-hand panel rotates this view through 90° to better visualise the relative reorientation of W306 and F164, and the outward displacement of M4. This expands the K2P modulator site behind the selectivity filter (red asterisk).

Figure 5. Extracellular inhibition of TREK-2 by Nb-Inhibitor-61. **(A)** Dose-response relationships showing inhibition of TREK-2 channel activity by Nb-Inhibitor-61 (Nb61). Whole-cell TREK-2 currents were recorded at +40 mV and perfused with different concentrations of Nb67. Also shown are the effect of different mutations of K103 in Nb61. **(B)** The crystal structure unit cell reveals only one Nb61 bound to TREK-2; packing interactions between the Cap domains within the crystal prevent binding to the other side. **(C)** Expanded view of the major interactions of Nb61 with the top of M3 and the M3-PH2. Additional interactions with the P2-M4 loop and M2 are also observed **(D)** Expanded view of interactions between Nb61 and the side of the Cap domain. **(E)** Surface view showing obstruction of the extracellular ion exit pathway by Nb61 (in purple). K103 within the obstructed pathway is also marked (in red). (**F**). Expanded view of the location of K103 within the ion exit pathway. K^+ ions are shown as purple spheres and the arrows indicate the direction of K^+ flow through the ion exit pathway that is obstructed by K103 on CDR3 of Nb61.

Figure 6. Engineering of a high-affinity biparatropic inhibitory nanobody. **(A)** Dose-response relationships showing inhibition of TREK-2 channel activity by the divalent linked Nb-Inhibitor-6158 (Nb61). Whole-cell TREK-2 currents were recorded at +40 mV and perfused with different concentrations Nb6158. Consistent with its markedly increased affinity, this linked nanobody exhibits a marked increase in its inhibitory efficacy compared to Nb61 alone. **(B)** A 7.4Å resolution CryoEM structure of TREK-2 in complex with Nb6158 shows two copies of Nb61 bound, one to each side of the Cap domain. An expanded view of their relative position is shown on the right. This indicates that, in addition to any allosteric effects, Nb61 is capable of interacting with TREK2 on both sides of the Cap domain to obstruct K^+ permeation from both extracellular ion exit pathways.

Figure 7. Activation and Inhibition by opposite movement of the top of M4. Alignment of the TREK-2/Nb76 and TREK-2/Nb61 complexes with the TREK-2 Up state show that activation by Nb76 is associated with outward movement of the top of M4 and the P2-M4 loop whilst inhibition by Nb61 involves movement in the opposite direction (red arrows). The location of the K2P modulator site behind the selectivity filter is indicated by the asterisk.

References

1. Bagal SK*, et al.* Ion channels as therapeutic targets: a drug discovery perspective. *J Med Chem* **56**, 593-624 (2013).
2. Mathie A*, et al.* Two-Pore Domain Potassium Channels as Drug Targets: Anesthesia and Beyond. *Annu Rev Pharmacol Toxicol* **61**, 401-420 (2021).
3. Mathie A*, et al.* Pharmacological Approaches to Studying Potassium Channels. *Handb Exp Pharmacol* **267**, 83-111 (2021).
4. Schewe M*, et al.* A pharmacological master key mechanism that unlocks the selectivity filter gate in K(+) channels. *Science* **363**, 875-880 (2019).
5. Enyedi P, Czirjak G. Molecular background of leak K+ currents: two-pore domain potassium channels. *Physiol Rev* **90**, 559-605 (2010).
6. Niemeyer MI, Cid LP, Gonzalez W, Sepulveda FV. Gating, Regulation, and Structure in K2P K+ Channels: In Varietate Concordia? *Mol Pharmacol* **90**, 309-317 (2016).
7. Natale AM, Deal PE, Minor DL, Jr. Structural insights into the mechanisms and pharmacology of K2P potassium channels. *J Mol Biol*, 166995 (2021).
8. Brohawn SG, Campbell EB, MacKinnon R. Physical mechanism for gating and mechanosensitivity of the human TRAAK K+ channel. *Nature* **516**, 126-130 (2014).
9. Dong YY*, et al.* K2P channel gating mechanisms revealed by structures of TREK-2 and a complex with Prozac. *Science* **347**, 1256-1259 (2015).
10. Schmidpeter PAM*, et al.* Membrane phospholipids control gating of the mechanosensitive potassium leak channel TREK1. *Nat Commun* **14**, 1077 (2023).
11. Lolicato M*, et al.* K2P channel C-type gating involves asymmetric selectivity filter order-disorder transitions. *Science Advances* **6**, eabc9174. (2020).
12. McClenaghan C*, et al.* Polymodal activation of the TREK-2 K2P channel produces structurally distinct open states. *J Gen Physiol* **147**, 497-505 (2016).
13. Proks P*, et al.* Multiple Mechanisms Underlie State-Independent Inhibitory Effects of Norfluoxetine on TREK-2 K2P Channels. *bioRxiv*, 2020.2010.2029.360966 (2021).
14. Türkaydin B*, et al.* From head to tail - Atomistic mechanism of long-range coupling from the cytosolic sensor domain to the selectivity filter in TREK K_{2P} channels. *bioRxiv*, 2023.2010.2006.561191 (2023).
15. Busserolles J*, et al.* TREK1 channel activation as a new analgesic strategy devoid of opioid adverse effects. *Br J Pharmacol* **177**, 4782-4795 (2020).
16. Lolicato M*, et al.* K2P2.1 (TREK-1)-activator complexes reveal a cryptic selectivity filter binding site. *Nature* **547**, 364-368 (2017).
17. Huang Z, Niu L. Developing RNA aptamers for potential treatment of neurological diseases. *Future Med Chem* **11**, 551-565 (2019).
18. Zhao Y*, et al.* Toxins Targeting the Kv1.3 Channel: Potential Immunomodulators for Autoimmune Diseases. *Toxins (Basel)* **7**, 1749-1764 (2015).
19. Colecraft HM, Trimmer JS. Controlling ion channel function with renewable recombinant antibodies. *J Physiol* **600**, 2023-2036 (2022).

20. Tiede C*, et al.* Affimer proteins are versatile and renewable affinity reagents. *Elife* **6**, (2017).
21. Wulff H*, et al.* Antibodies and venom peptides: new modalities for ion channels. *Nat Rev Drug Discov* **18**, 339-357 (2019).
22. Selvakumar P*, et al.* Structures of the T cell potassium channel Kv1.3 with immunoglobulin modulators. *Nat Commun* **13**, 3854 (2022).
23. Zhu Y, Wang SS, Zhou ZS, Ho M. The emergence of AntibodyPlus: the future trend of antibody-based therapeutics. *Antib Ther* **5**, 280-287 (2022).
24. Muyldermans S. Nanobodies: natural single-domain antibodies. *Annu Rev Biochem* **82**, 775-797 (2013).
25. Stortelers C, Pinto-Espinoza C, Van Hoorick D, Koch-Nolte F. Modulating ion channel function with antibodies and nanobodies. *Curr Opin Immunol* **52**, 18-26 (2018).
26. De Genst E*, et al.* Molecular basis for the preferential cleft recognition by dromedary heavy-chain antibodies. *Proc Natl Acad Sci U S A* **103**, 4586-4591 (2006).
27. Steeland S, Vandenbroucke RE, Libert C. Nanobodies as therapeutics: big opportunities for small antibodies. *Drug Discov Today* **21**, 1076-1113 (2016).
28. Muyldermans S. Applications of Nanobodies. *Annu Rev Anim Biosci* **9**, 401-421 (2021).
29. Uchanski T, Pardon E, Steyaert J. Nanobodies to study protein conformational states. *Curr Opin Struct Biol* **60**, 117-123 (2020).
30. Pardon E*, et al.* A general protocol for the generation of Nanobodies for structural biology. *Nat Protoc* **9**, 674-693 (2014).
31. Wiedmann F*, et al.* N-Glycosylation of TREK-1/hK(2P)2.1 Two-Pore-Domain Potassium (K(2P)) Channels. *Int J Mol Sci* **20**, (2019).
32. Sandoz G*, et al.* Extracellular acidification exerts opposite actions on TREK1 and TREK2 potassium channels via a single conserved histidine residue. *Proc Natl Acad Sci U S A* **106**, 14628-14633 (2009).
33. Brohawn SG, del Marmol J, MacKinnon R. Crystal structure of the human K2P TRAAK, a lipid- and mechano-sensitive K+ ion channel. *Science* **335**, 436-441 (2012).
34. Deal P*, et al.* Development of covalent chemogenetic K2P channel activators. *bioRxiv*, 2023.2010.2015.561774 (2023).
35. Lolicato M*, et al.* Transmembrane helix straightening and buckling underlies activation of mechanosensitive and thermosensitive K(2P) channels. *Neuron* **84**, 1198-1212 (2014).
36. Pope L, Minor DL, Jr. The Polysite Pharmacology of TREK K(2P) Channels. *Adv Exp Med Biol* **1349**, 51-65 (2021).
37. Banerjee A, Lee A, Campbell E, Mackinnon R. Structure of a pore-blocking toxin in complex with a eukaryotic voltage-dependent K(+) channel. *Elife* **2**, e00594 (2013).
38. Pope L, Lolicato M, Minor DL, Jr. Polynuclear Ruthenium Amines Inhibit K2P Channels via a "Finger in the Dam" Mechanism. *Cell Chem Biol* **27**, 511-524 e514 (2020).
39. Karbat I*, et al.* Pore-modulating toxins exploit inherent slow inactivation to block K(+) channels. *Proc Natl Acad Sci U S A* **116**, 18700-18709 (2019).
40. Saikia C*, et al.* A Molecular Lid Mechanism of K(+) Channel Blocker Action Revealed by a Cone Peptide. *J Mol Biol* **433**, 166957 (2021).

41. Wagner TR, *et al.* Biparatopic nanobodies protect mice from lethal challenge with SARS-CoV-2 variants of concern. *EMBO Rep* **23**, e53865 (2022).
42. Walter JD, *et al.* Biparatopic sybodies neutralize SARS-CoV-2 variants of concern and mitigate drug resistance. *EMBO Rep* **23**, e54199 (2022).
43. Miller AN, Long SB. Crystal structure of the human two-pore domain potassium channel K2P1. *Science* **335**, 432-436 (2012).
44. Chen Z, *et al.* A single conserved basic residue in the potassium channel filter region controls KCNQ1 insensitivity toward scorpion toxins. *Biochem Biophys Rep* **3**, 62-67 (2015).
45. Kabsch W. Xds. *Acta Crystallogr D Biol Crystallogr* **66**, 125-132 (2010).
46. Evans P. Scaling and assessment of data quality. *Acta Crystallogr D Biol Crystallogr* **62**, 72-82 (2006).
47. Smart OS, *et al.* Exploiting structure similarity in refinement: automated NCS and target-structure restraints in BUSTER. *Acta Crystallogr D Biol Crystallogr* **68**, 368-380 (2012).
48. Caesar J, *et al.* SIMPLE 3.0. Stream single-particle cryo-EM analysis in real time. *J Struct Biol X* **4**, 100040 (2020).
49. Punjani A, Rubinstein JL, Fleet DJ, Brubaker MA. cryoSPARC: algorithms for rapid unsupervised cryo-EM structure determination. *Nat Methods* **14**, 290-296 (2017).
50. Emsley P, Lohkamp B, Scott WG, Cowtan K. Features and development of Coot. *Acta Crystallogr D Biol Crystallogr* **66**, 486-501 (2010).
51. Adams PD, *et al.* PHENIX: a comprehensive Python-based system for macromolecular structure solution. *Acta Crystallogr D Biol Crystallogr* **66**, 213-221 (2010).

Figure 1

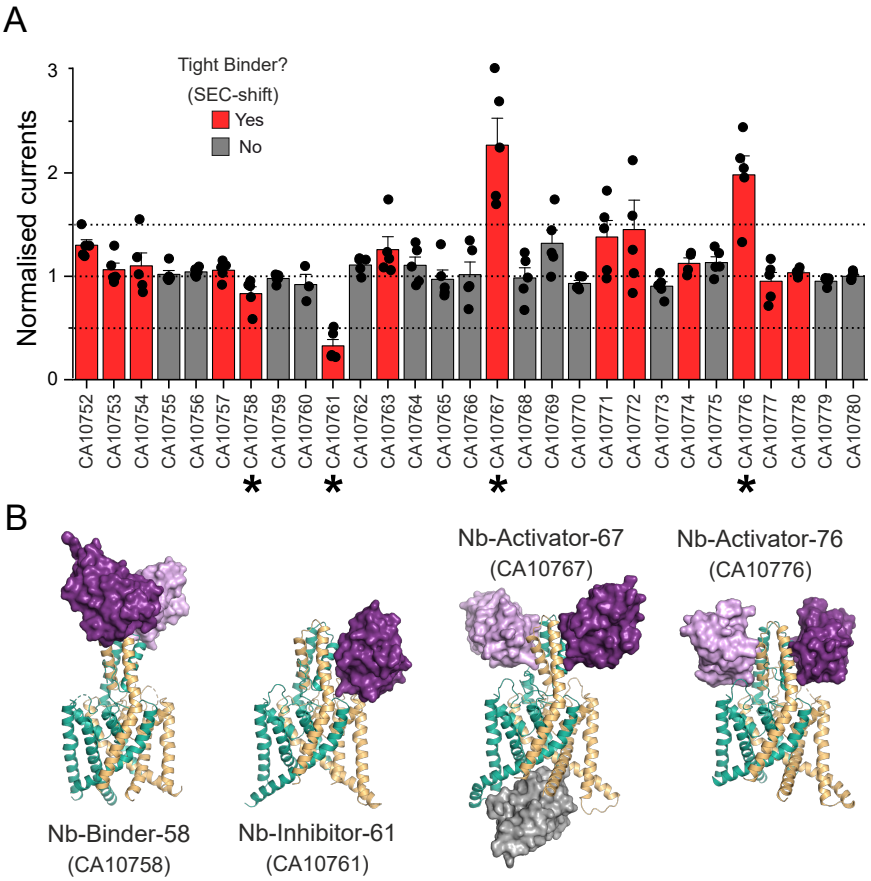
A
Tight Binder?
(SEC-shift)
Yes
No
Normalised currents
0
1
2
3
CA10752
CA10753
CA10754
CA10755
CA10756
CA10757
CA10758
CA10759
CA10760
CA10761
CA10762
CA10763
CA10764
CA10765
CA10766
CA10767
CA10768
CA10769
CA10770
CA10771
CA10772
CA10773
CA10774
CA10775
CA10776
CA10777
CA10778
CA10779
CA10780
*
*
*
*
B
Nb-Binder-58
(CA10758)
Nb-Inhibitor-61
(CA10761)
Nb-Activator-67
(CA10767)
Nb-Activator-76
(CA10776)

Figure 2

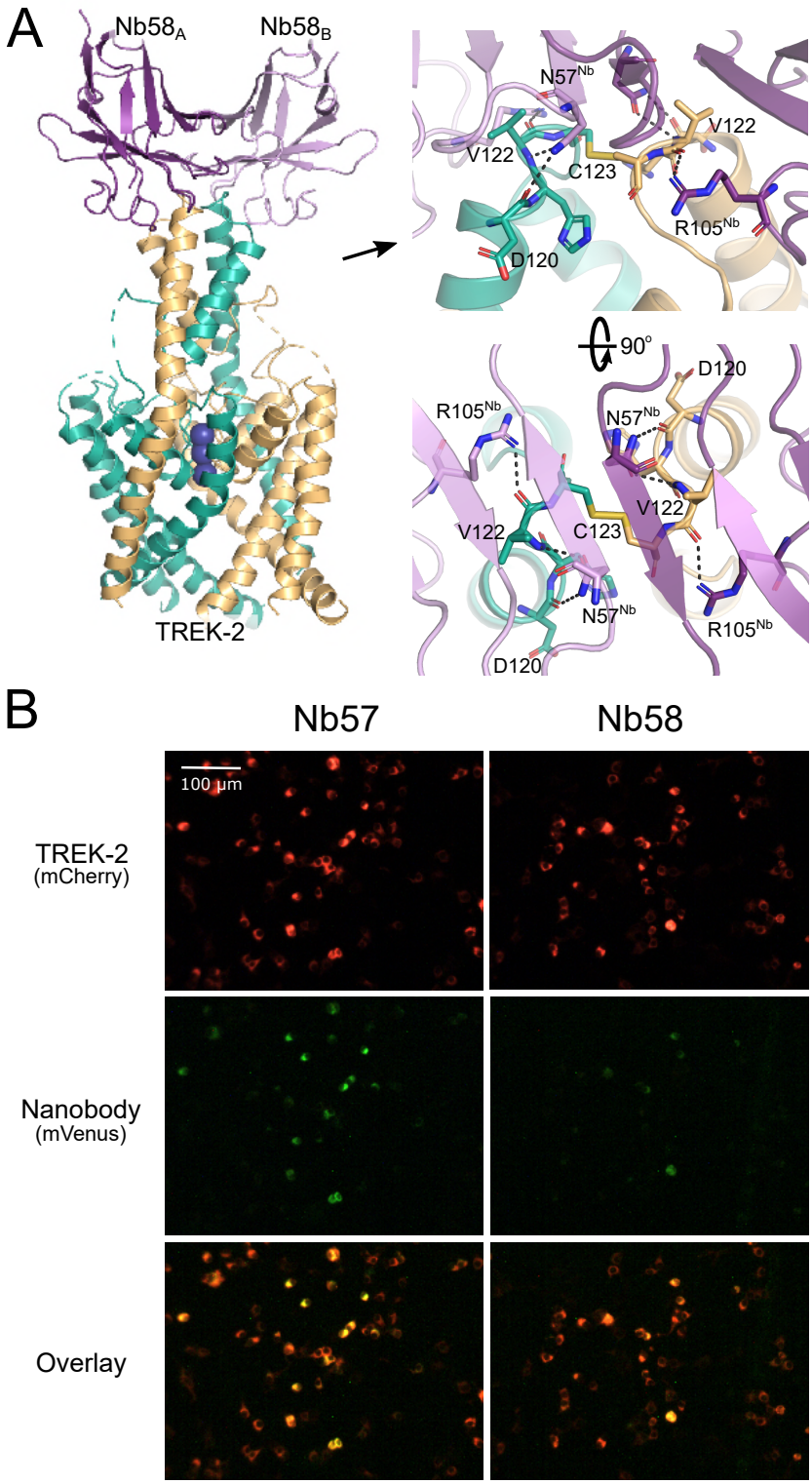
A
Nb58A
Nb58B
TREK-2
N57Nb
V122
C123
V122
R105Nb
D120
90°
D120
R105Nb
N57Nb
V122
V122
C123
N57Nb
R105Nb
D120
B
Nb57
Nb58
100 µm
TREK-2
(mCherry)
Nanobody
(mVenus)
Overlay

Figure 3

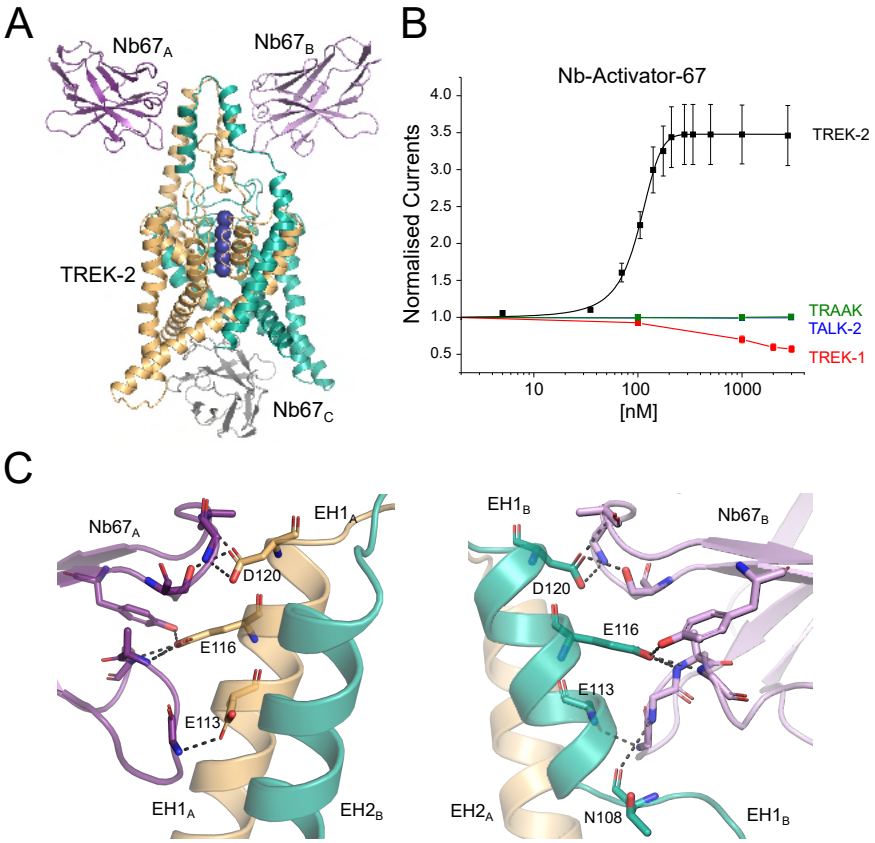
A
Nb67A
Nb67B
TREK-2
Nb67C
B
Nb-Activator-67
Normalised Currents
4.0
3.5
3.0
2.5
2.0
1.5
1.0
0.5
10
100
1000
[nM]
TREK-2
TRAAK
TALK-2
TREK-1
C
Nb67A
EH1A
D120
E116
E113
EH1A
EH2B
EH1B
Nb67B
D120
E116
E113
EH2A
N108
EH1B

Figure 4

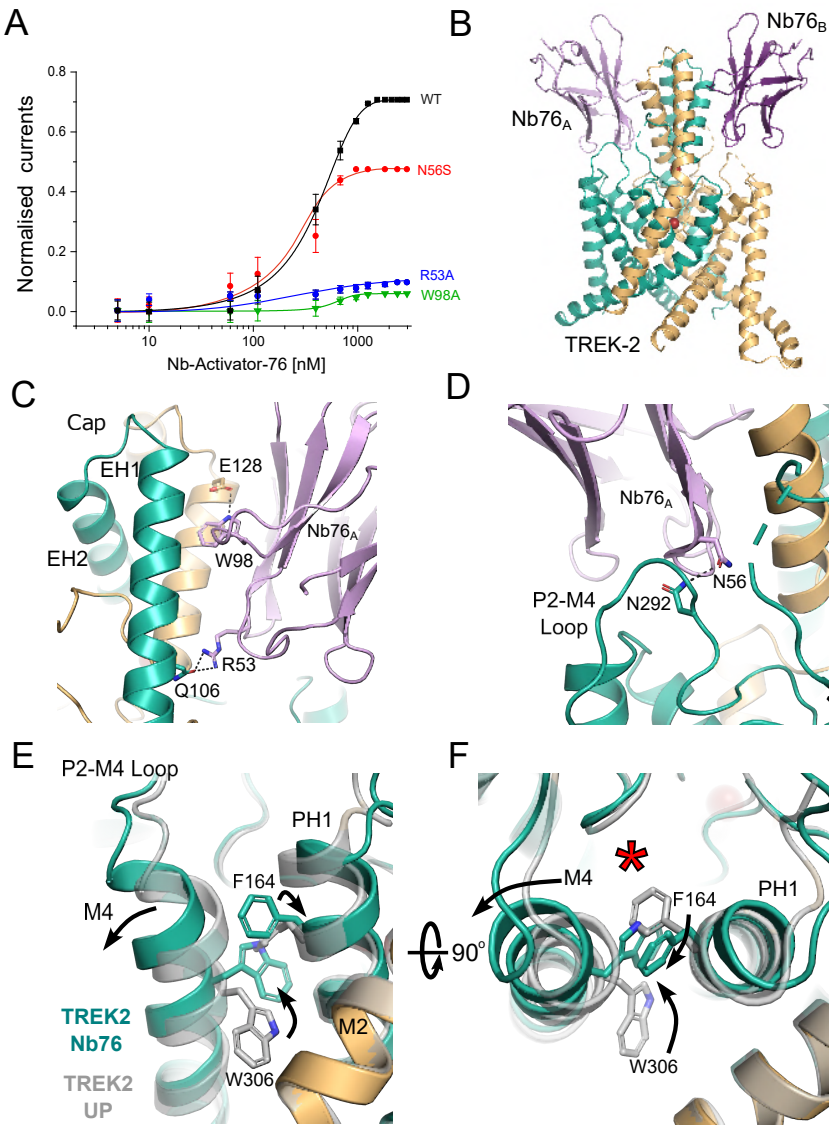
A
Normalised currents
0.8
0.6
0.4
0.2
0.0
10
100
1000
Nb-Activator-76 [nM]
WT
N56S
R53A
W98A
B
Nb76B
Nb76A
TREK-2
C
Cap
EH1
E128
Nb76A
EH2
W98
R53
Q106
D
Nb76A
N56
P2-M4
Loop
N292
E
P2-M4 Loop
PH1
F164
M4
TREK2
Nb76
TREK2
UP
M2
W306
F
M4
F164
PH1
90°
W306

Figure 5

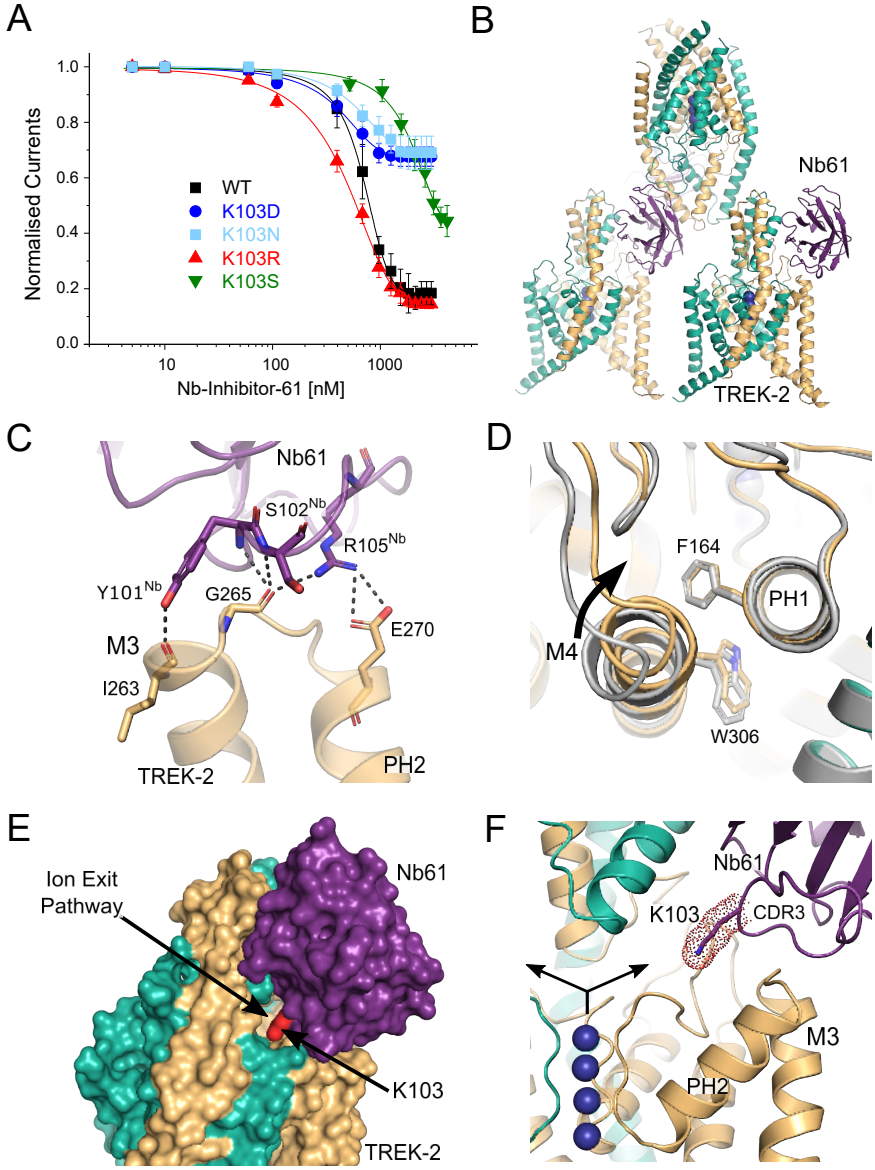
A
Normalised Currents
1.0
0.8
0.6
0.4
0.2
0.0
10
100
1000
Nb-Inhibitor-61 [nM]
WT
K103D
K103N
K103R
K103S
B
Nb61
TREK-2
C
Nb61
S102Nb
R105Nb
Y101Nb
G265
E270
M3
I263
TREK-2
PH2
D
F164
PH1
M4
W306
E
Ion Exit
Pathway
Nb61
K103
TREK-2
F
Nb61
K103
CDR3
M3
PH2

Figure 6

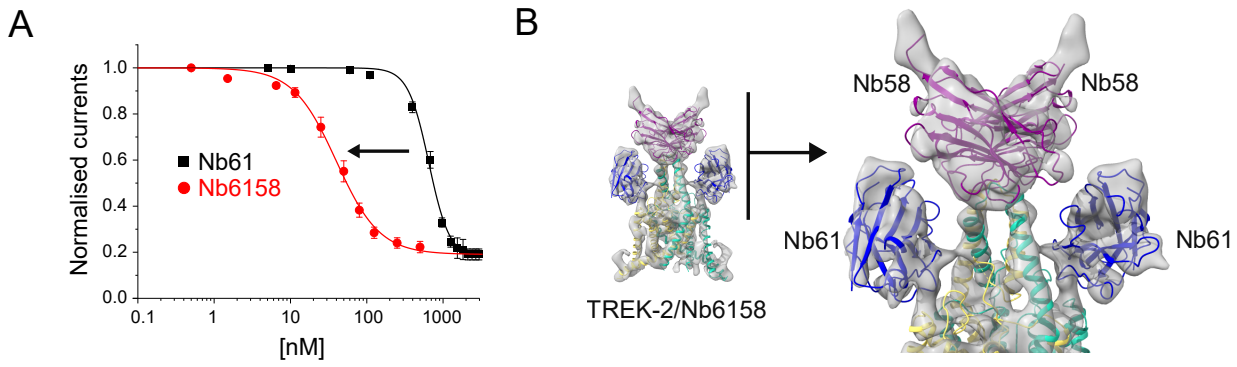
A
Normalised currents
1.0
0.8
0.6
0.4
0.2
0.0
0.1
1
10
100
1000
[nM]
Nb61
Nb6158
B
TREK-2/Nb6158
Nb58
Nb58
Nb61
Nb61

Figure 7

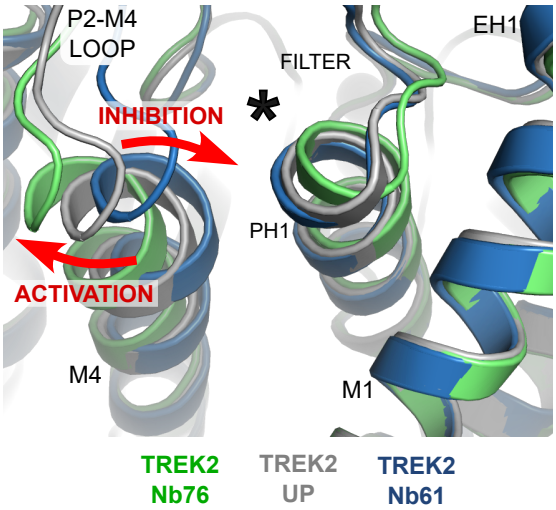
P2-M4
LOOP
INHIBITION
ACTIVATION
M4
FILTER
PH1
EH1
M1
TREK2
Nb76
TREK2
UP
TREK2
Nb61

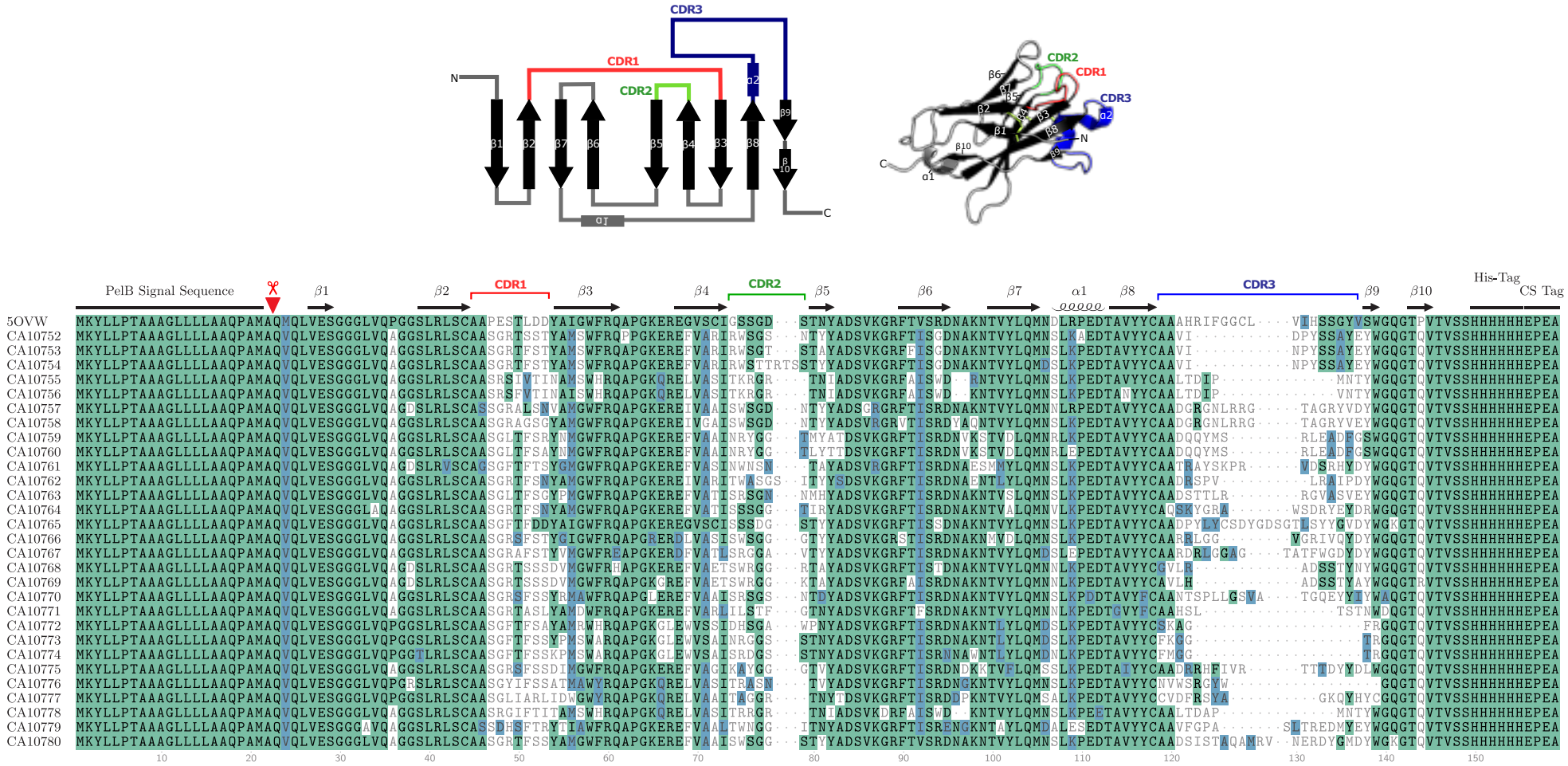

Figure S1 (Top) Cartoon description of a typical nanobody structure (that shown is PDB: 5OVW) indicating the β-sheet structure and CDR loops. Adjacent is a structure with each of the CDR loops coloured differently. Below is a sequence alignment with the TREK-2 nanobodies used in this study. The β-sheets, CDR1, CDR2 and CDR3 loops are highlighted. The PelB signal sequence for periplasmic secretion and His-Tag for purification are also included in these sequences. The purified nanobodies are cleaved at the position indicated (red inverted triangle and scissors). The numbering of residues within each nanobody therefore starts from this point.

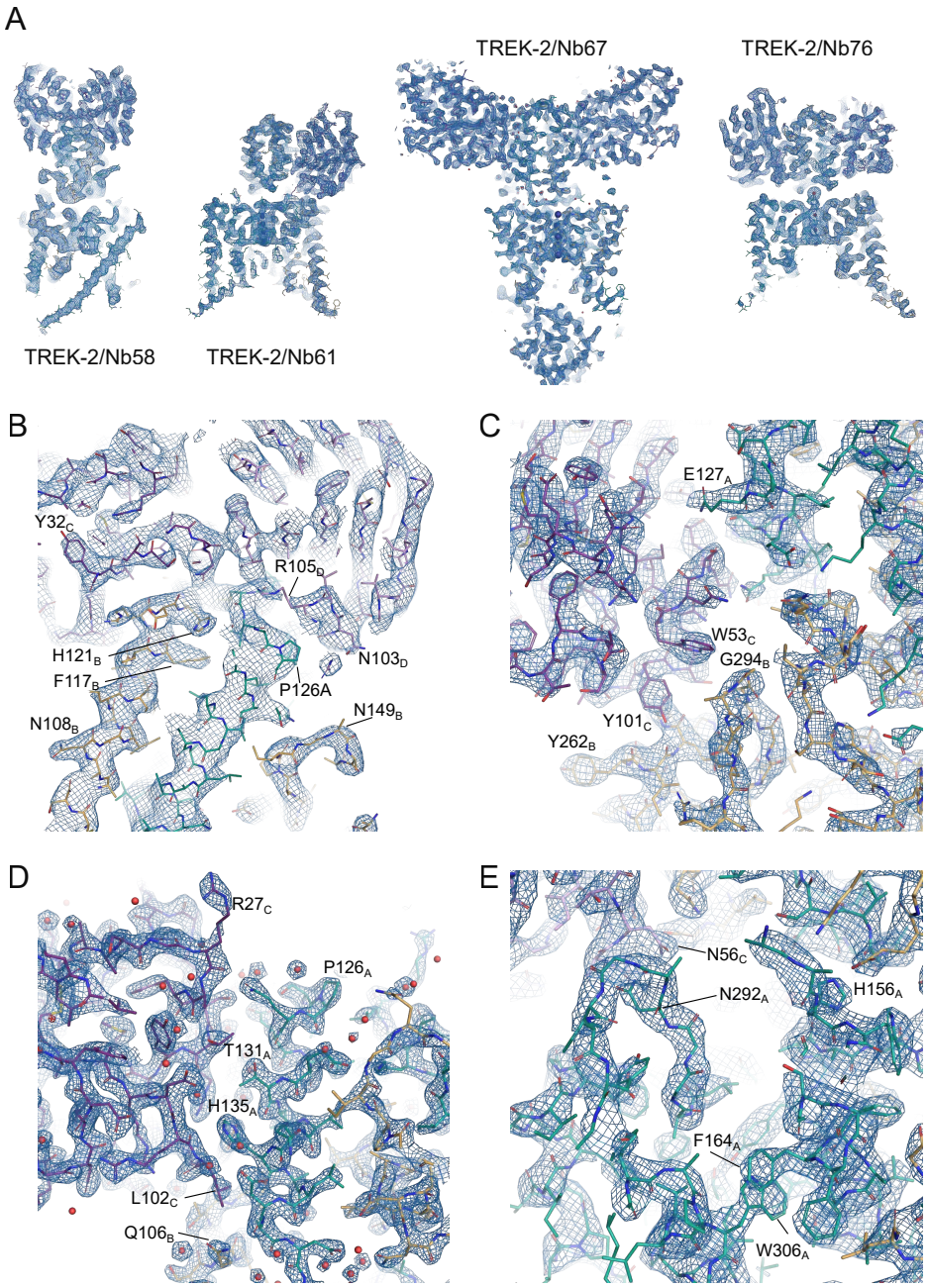

Figure S2. Quality of electron density for different TREK-2/nanobody complexes. **A**) Slice though of density for the four structures indicated. **B**) Interactions of Nb-Binder-58 with the Cap domain of TREK-2. C) Interactions of Nb-Inhibitor-61 with the top of M3 and the Cap domain. **D**) Interactions of Nb-Activator-67 with the Cap domain. **E**) Interactions of Nb-Activator-76 with the P2-M4 loop and Cap domain.

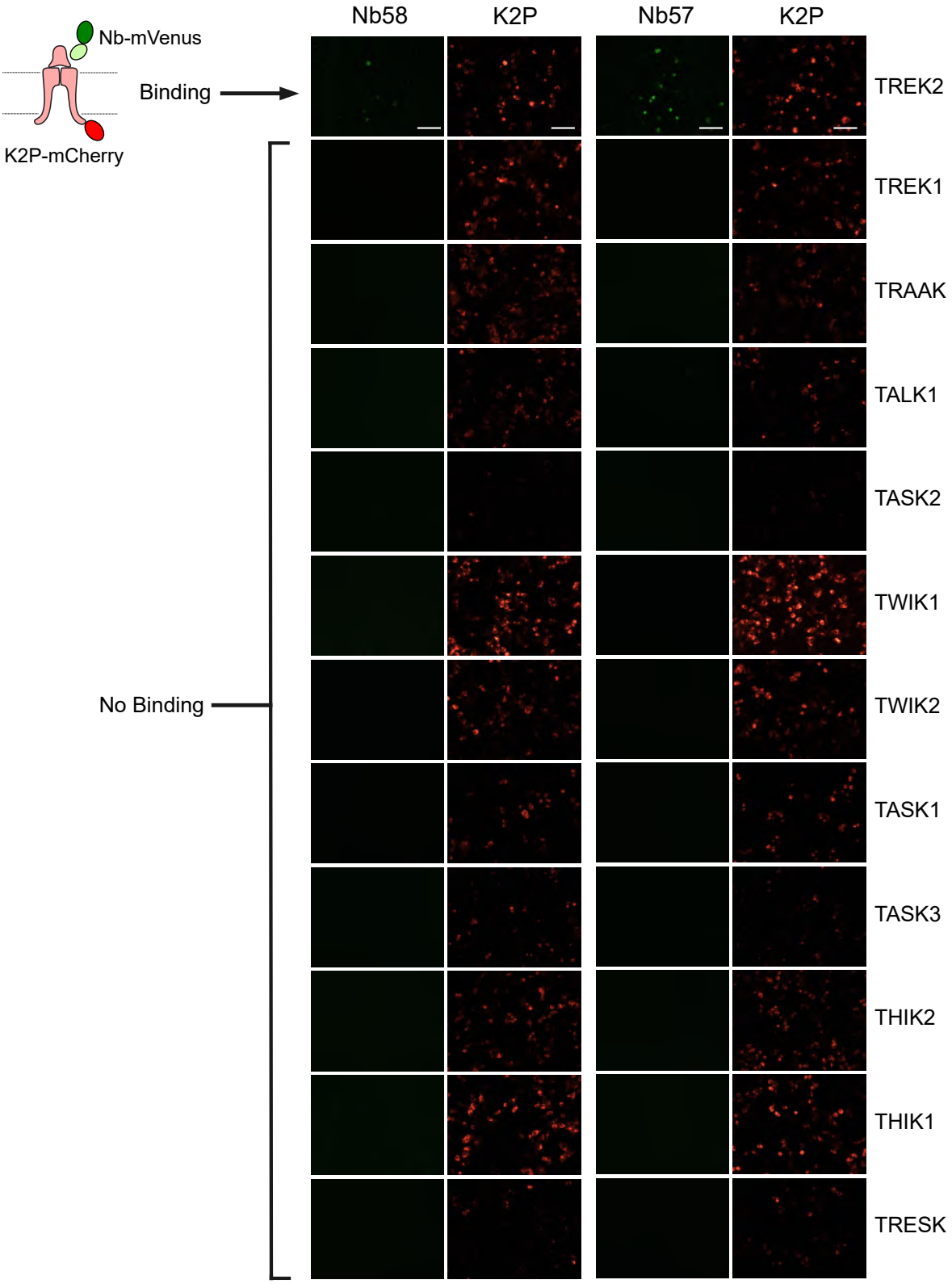

Figure S3. Extracellular nanobody binding to TREK-2 expressed in HEK293 cells. This data complements the data shown in Figure 2B and demonstrates the specificity of Nb57 and Nb58 binding to TREK-2 channels. The cartoon in the top left summarises the binding assay: the K2P channels are fused to mCherry and the nanobodies to mVenus. Binding is only detected with TREK2 and not with any of the other K2P channels tested. The overlays for Nb57 and Nb58 are shown in greater detail in Figure 2B.

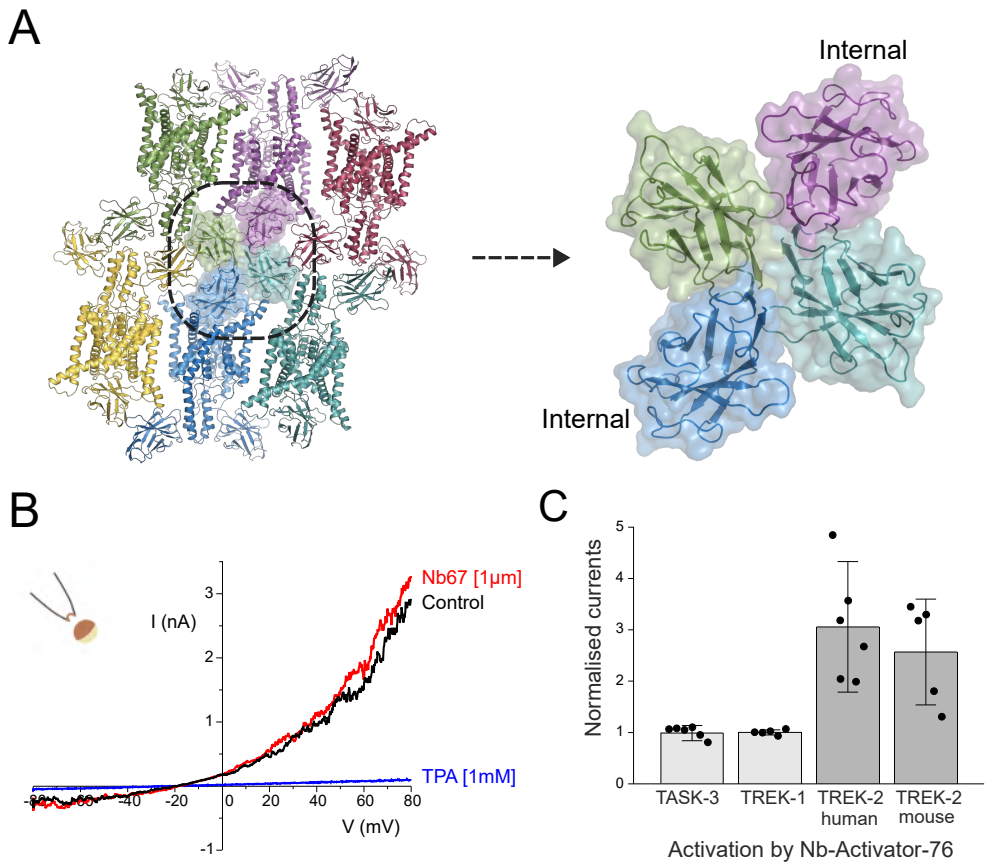

Figure S4. A) Crystal packing for the Nb67/TREK-2 complex showing that the 'internally' bound copy of Nb67 (blue/purple) forms tetramers with the extrenally bound copies within the unit cell. The area within this dotted line is expanded on the right-hand side showing this tetramerisation more clearly. **B**) Intracellular application of Nb67 has no functional effect. Nb67 was perfused onto the intracellular surface of giant patches excised form oocytes expressing TREK-2 channels. The same channels could be inhibited by intracellular application of tetrapentylammonium (TPA). **C**) Normalised whole-cell currents showing that Nb76 (1 μM) does not activate TASK-3 or TREK-1. However, marked activation of both human and mouse TREK-2 currents are observed.

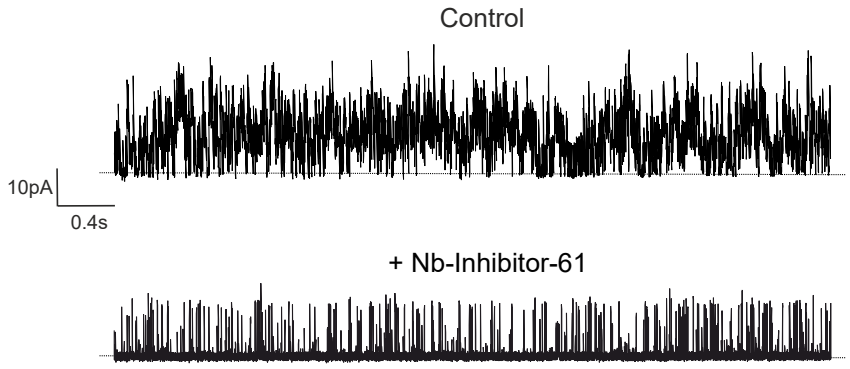

Figure S5. The effect of Nb-Inhibitor-61 on TREK-2 activity at the single channel level. Due to the low intrinsic open-probability of TREK-2, a qualitative comparison is shown above between the behaviour of multi-channel patches with (bottom) or without (top) Nb61 included in the pipette solution. Suppression of TREK-2 activity is seen by a reduction in the durations of bursts of openings, and increase in the time spent in the long closed states. This is consistent with the idea that this nanobody acts directly as a slow blocker resulting in a complete block of K^+ flux through the channel.

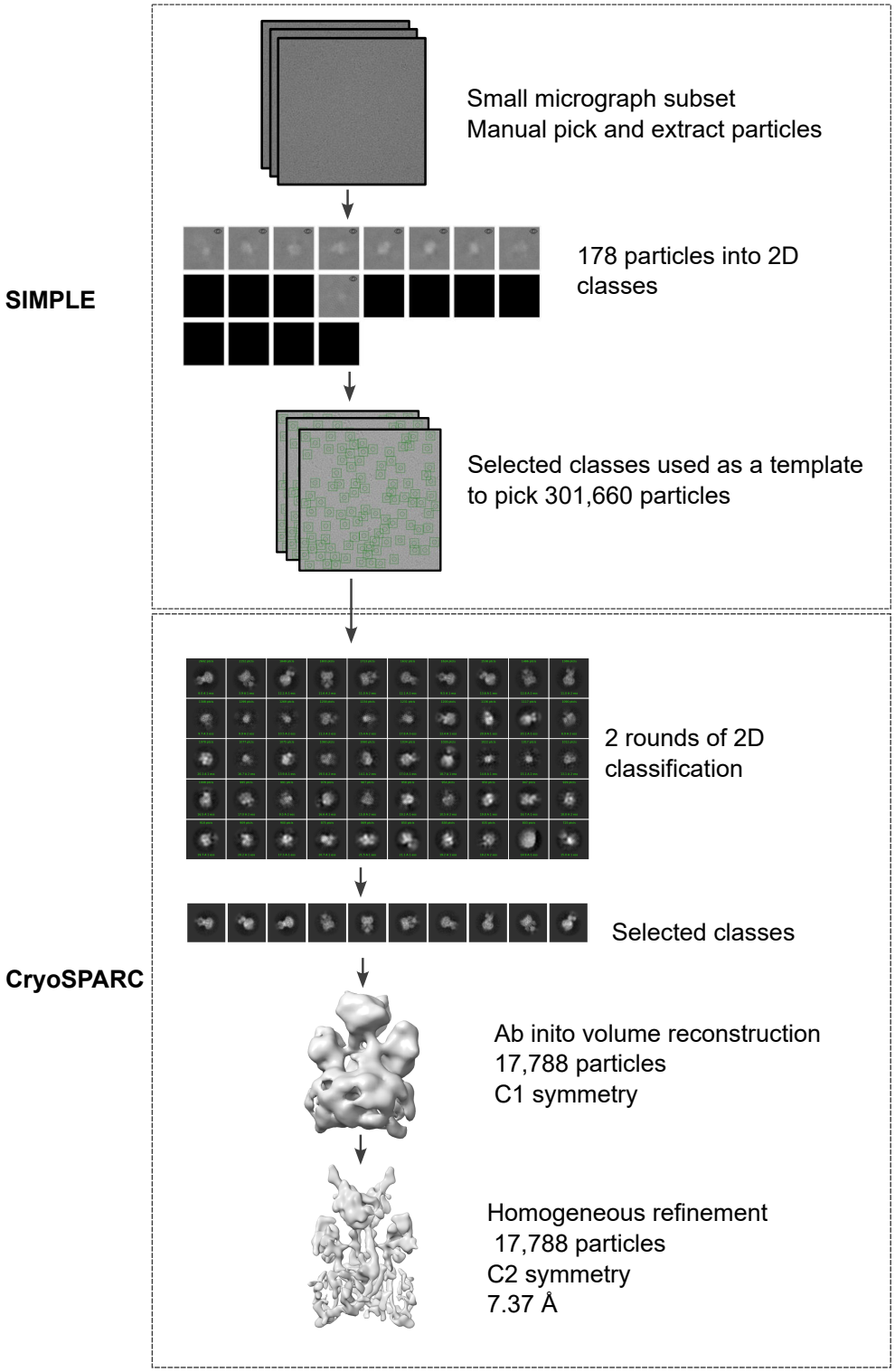

Figure S6. Flowchart for the single particle reconstruction of TREK-2 in complex with the biparatopic linked Nb-inhibitor-5861. Particles were picked and extracted in SIMPLE. 2D classification, volume reconstruction and refinement were carried out in CryoSPARC. The final reconstruction of 17,788 particles gave a map of resolution 7.37 Å.

Table S1. X-ray data collection and refinement statistics.

	TREK-2 Nb58 (8QZ1)	**TREK-2 Nb61 (8QZ2)**	**TREK-2 Nb67 (8QZ3)**	**TREK-2 Nb76 (8QZ4)**
Data collection				
Space group	H3	$C222_1$	$P22_12_1$	$P2_12_12_1$
Cell dimensions				
a, b, c (Å)	233.663, 233.663, 67.338	56.538, 111.698, 289.208	51.264, 102.100, 215.817	68.280, 75.756, 259.150
α, β, γ (°)	90, 90, 120	90, 90, 90	90, 90, 90	90, 90, 90
Resolution (Å)	44.16-3.59 (3.69-3.59)	57.84-3.50 (3.58-3.50)	58.81-2.40 (2.49-2.40)	51.83-3.20 (3.34-3.20)
No. reflections / unique	73,209 / 14,181	63,807 / 11,445	221,034 / 34,388	72,190 / 17,904
R_{pim}	0.051 (0.649)	0.223 (0.799)	0.087 (0.536)	0.066 (0.522)
R_{meas}	0.116 (1.339)	0.540 (1.997)	0.219 (1.363)	0.134 (1.065)
I/σI	8.6 (1.3)	3.7 (1.2)	6.3 (1.6)	8.4 (1.7)
Correlation coefficient ($CC_{1/2}$)	0.996 (0.511)	0.997 (0.488)	0.989 (0.610)	0.998 (0.615)
Completeness (%)	88.6 (55.7)	95.0 (79.7)	75.6 (35.9)	77.9 (34.4)
Multiplicity	5.2 (4.1)	5.6 (6.1)	6.4 (6.3)	4.0 (4.0)
Refinement				
Resolution (Å)	31.30-3.60	52.98-3.50	58.81-2.40	31.25-3.20
No. reflections	14,165	11,398	34,319	17,829
R_{work} / R_{free} (%)	25.51 / 29.84	27.95 / 30.82	27.75 / 29.09	27.04 / 29.84
No. atoms				
Protein	5132	4507	6878	5321
Ligand/ion	3	4	13	144
Water	-	-	191	8
B-factors				
Protein	154.18	65.65	44.79	76.08
Ligand/ion	138.86	41.13	47.07	144.17
Water	-	-	28.52	26.30
R.m.s. deviations				
Bond lengths (Å)	0.0053	0.0049	0.0046	0.0044
Bond angles (°)	0.708	0.684	0.679	0.655